ELSEVIER

Journal of Power Sources 53 (1995) 53–61

JOURNAL OF POWER SOURCES

Passivation and corrosion phenomena on lead–calcium–tin alloys of lead/acid battery positive electrodes

R. Miraglio [a], L. Albert [b], A. El Ghachcham [c], J. Steinmetz [d], J.P. Hilger [c]

[a] *CEAC, 18 quai de Clichy, B.P. 306, 92111 Clichy Cedex, France*

[b] *Metaleurop Recherche, 1 avenue A. Einstein, B.P. 120, 78193 Trappes, France*

[c] *Laboratoire de Thermodynamique Métallurgique, CNRS: ER 78, Université de Nancy I, B.P. 239, 54506 Vandoeuvre-lès-Nancy Cedex, France*

[d] *Laboratoire de Chimie du Solide Minéral, CNRS: URA 158, Université de Nancy I, B.P. 239, 54506 Vandoeuvre-lès-Nancy Cedex, France*

Received 21 September 1994; accepted 26 October 1994

Abstract

The corrosion behaviour of lead–calcium–tin alloys has been examined at two anodization potentials that correspond, respectively, to overcharge and to passivation by PbO conditions. The role of tin on the passivation phenomenon is examined in detail, while the evolution of hardening and microstructure is followed on the same samples, namely, grids (expanded and gravity cast) with different tin levels and strips, manufactured from primary or secondary lead.

Keywords: Lead–calcium–tin alloys; Lead/acid batteries; Passivation; Corrosion

1. Introduction

Most manufacturers of lead/acid batteries for applications such as the starting, lighting and ignition (SLI) of vehicles have opted for lead–calcium–tin ternary alloys. In this case, the tin content must be controlled at a level that is sufficient to avoid the development of a high impedance 'passivation' layer of lead monoxide at the grid/active-material interface. It is known, for example, that an addition of 0.2–0.4 wt.% Sn is effective in preventing the formation of α-PbO [1].

The work reported here relates some experiences carried out on alloys with different amounts of tin (up to 2 wt.%) in order to determine the 'active element' limit from which the passivation phenomenon is suppressed, in relation also with the substrate structure. On the other hand, accelerated tests have been developed to measure the influence of both the purity and the metallurgical treatment of the lead on the corrosion due to the overcharge.

2. Experimental

2.1. Preparation of samples

The lead–calcium–tin (Pb–Ca–Sn) alloys selected for this study are listed in Table 1. Alloys denoted S_1 to S_8 have been prepared in the form of small strips (13 cm × 7 cm × 0.7 cm and 13 cm × 7 cm × 0.3 cm) at Trappes Research Center of Metaleurop. Two moulds made of copper (one for the 0.7 cm thick strips, and a second for the thinner strips) were used to reproduce on a laboratory scale, as close as possible, the high cooling rates experienced in the industrial manufacture of battery grids (gravity casting only). The dimensions of the moulds were evaluated by taking into account only the conductive heat transfer from liquid metal to the walls. A maximum cooling rate of about 60–70 °C per second was anticipated but, in practice, experimental cooling rates were nearer to 40 °C s^{-1} than 70 °C s^{-1}.

Four different alloy configurations were prepared (composition: Pb–0.1wt.%Ca–0.6wt.%Sn–0.01 to 0.02 wt.%Al), namely: (i) a basaltic structure with electrolytic primary lead; (ii) equiaxed grains structure with electrolytic primary lead; (iii) a basaltic structure with secondary lead; (iv) equiaxed grains structure with secondary lead. The basaltic structure was obtained by pouring the liquid mixture at 600 °C into a mould that was maintained at ambient temperature and by quenching the strip into water just after solidification. By contrast, the equiaxed structure was obtained by pouring at the same temperature into a mould preheated to 200 °C, then cooling the strips in ambient air immediately after solidification.

SSDI 0378-7753(94)02153-T

Table 1
Compositions and characteristics of Pb–Ca–Sn alloys

	Composition (wt.%)								Characteristics			
	Ca (%)	Sn (%)	Al ($\times 10^{-4}$%)	Bi ($\times 10^{-4}$%)	Ag ($\times 10^{-4}$%)	Cu ($\times 10^{-4}$%)	Te ($\times 10^{-4}$%)	Sn/Ca	Thickness (mm)	Mould temperature (°C)	Structure	Hardness HV2
Strips												
Plate S_1												
Primary lead	0.100	0.58	169	20	1	4	1	6	3	20	basaltic	14.3
Plate S_2												
Primary lead	0.097	0.58	131	20	1	4	1	6	7	20	basaltic	15.2
Plate S_3												
Primary lead	0.094	0.57	138	20	1	4	1	6	3	200	equiaxed	14.4
Plate S_4												
Primary lead	0.094	0.57	158	20	1	4	1	6	7	200	equiaxed	14.6
Plate S_5												
Secondary lead	0.103	0.60	149	277	31	5	1	6	3	20	basaltic	14.9
Plate S_6												
Secondary lead	0.103	0.60	149	277	31	5	1	6	7	20	basaltic	15.8
Plate S_7												
Secondary lead	0.122	0.61	160	284	31	5	1	6	3	200	equiaxed	15.3
Plate S_8												
Secondary lead	0.122	0.61	160	284	31	5	1	6	7	200	equiaxed	14.3
Gravity cast grids												HV
G_1	0.100	0.56	140					6				17.8
G_2	0.095	1.24	130					13				18.7
G_3	0.092	1.62	140					18				18.6
G_4	0.091	2.5	120					27				18.4
G_5	0.082	5.3	131					65				
Expanded grids												$HV = R(\text{MPa}) \times 0.3$
G_6	0.075	0.075	100–150					1				10
G_7	0.075	0.23	100–150					3				10.5
G_8	0.075	0.71	100–150					10				17.5
G_9	0.075	1.18	100–150					16				19
G_{10}	0.075	2.16	100–150					29				19

Samples denoted G_1–G_{10} in Table 1 were produced under industrial conditions. G_1–G_5 grids were cast by gravity in a small industrial book-mould that was assigned specifically to these experiments. The mould was a TBS design located at the Florival CEAC Plant (Belgium). The grids were traditional SLI types and were produced at a rate of 13–14 (in a double form) per minute. Investigations showed that appropriate temperatures were: (i) furnace, 520 °C; (ii) foundry ladle, 545 °C; (iii) mould, 180 °C. The furnace capacity was 700 kg of lead alloy.

G_6–G_{10} alloys were rolled to 90% and expanded on an industrial machine (Properzi, Romano CEAC Plant in Italy).

Vickers tests were carried out on both the S series samples and the G grids (G_1–G_5), after ageing, whereas ultimate strength and elongation were followed during 90 days on the G_6–G_{10} grids.

2.2. Electrochemical tests

The following two types of experiments were carried out on the alloys.

(i) Accelerated corrosion tests performed in 5 M H_2SO_4 (50 °C) at an applied potential of 1.5 V in order to study the overcharge over a maximum period of one week. All the potentials were measured and are reported versus an Hg/Hg_2SO_4, K_2SO_4 saturated reference electrode. At regular intervals, grids (G_1–G_{10}) were weighed (after complete dissolution of the corrosion products in a mixture that contained CH_3COOH and N_2H_4). The plots of weight loss versus time, associated with microscope observations, allowed measurement of the degree of corrosion. After accelerated corrosion tests, samples of the S series were embedded in holders, polished with SiC paper (1000 grade), diamond paste (6 and 1 μm) and alumina (0.05 μm). Then, they were chemically attacked with a mixture of CH_3COOH and H_2O_2 (in a volume of 3 to 1, respectively). They were also analyzed by electron-probe microanalysis (EPMA) using a CAMECA SX50 instrument.

(ii) Corrosion tests performed in 0.5 M H_2SO_4 (20 °C), in the dark, at an applied potential of 0.7 V for passivation studies. After the grids were anodized for 24 h, voltammograms were run for scans carried out at a sweep rate of 1 mV s^{-1} and limited by the potential values:

$$(+0.7 \longrightarrow \underset{\text{scan 1}}{+1.6} \longrightarrow -1.6\ \text{V}) \longrightarrow$$

$$(+1.6 \longrightarrow \underset{\text{scan 2}}{-1.6\ \text{V}}) \longrightarrow (+1.6 \longrightarrow \underset{\text{scan 3}}{-1.6\ \text{V})}$$

During the first scan, the oxidation current of water at 1.4 V and the amount of PbO_2 reduced to $PbSO_4$ (measured by the corresponding peak area) depended closely on the conductivity of the PbO layer. At the end of the first cycle, all the lead contained in the corrosion product is transformed into a metallic form. Thus, during the next scan, both the water-oxidation current and the peak area associated with the reduction of PbO_2 to $PbSO_4$ increase. Scans 2 and 3 result in voltammograms that are very similar.

Two passivation criteria have been investigated. These are denoted by R and C. Namely: R is the intensity ratio of the water oxidation peak according to:

$$R = \frac{I_3\ (\text{mA}) \text{ for the third scan at } 1400\ \text{mV}}{I_1\ (\text{mA}) \text{ for the first scan at } 1400\ \text{mV}}$$

C is the peak area (P) ratio corresponding to PbO_2 reduction to $PbSO_4$

$$C = \frac{P_3 \text{ for the third scan}}{P_1 \text{ for the first scan}}$$

Consequently, when R and C values are close to 1, the corrosion layer, mainly constituted by PbO, is supposed to be more conductive, and the passivation is suppressed.

On the other hand, three expanded grids with different tin contents (0.23, 0.71 and 1.24 wt.%), as well as the S-series samples, were anodized for 5–7 days. The superficial phases were characterized by X-ray diffraction, while the metallographical cross sections were prepared for analysis by EPMA by applying the following conditions:

- primary voltage 15 kV
- beam current 10 nA
- matrix correction: PAP programme [2]
- standards: Pb ($PbSO_4$), Sn (pure metal), Ca ($CaSiO_3$), S ($PbSO_4$)
- counting time (s): $10 < t < 30$
- sample preparation: polishing and metallization (C)

3. Results

3.1. Microstructure, hardening processes and mechanical properties

The metallographical cross sections of the eight alloys of the S series are presented in the Figs. 1 and 2. They show a casting structure that nearly depends on the solidification rate. This parameter is related to the thickness of the strip and more strongly to the mould temperature.

All the cast samples harden according to a mechanism of discontinuous transformation. Thus, in some cases, two structures (casting and transformed) can be observed. For example, Fig. 1(d) shows a 'memory' of the as-cast dentritic structure that is superimposed on the puzzled structure that results from the successive

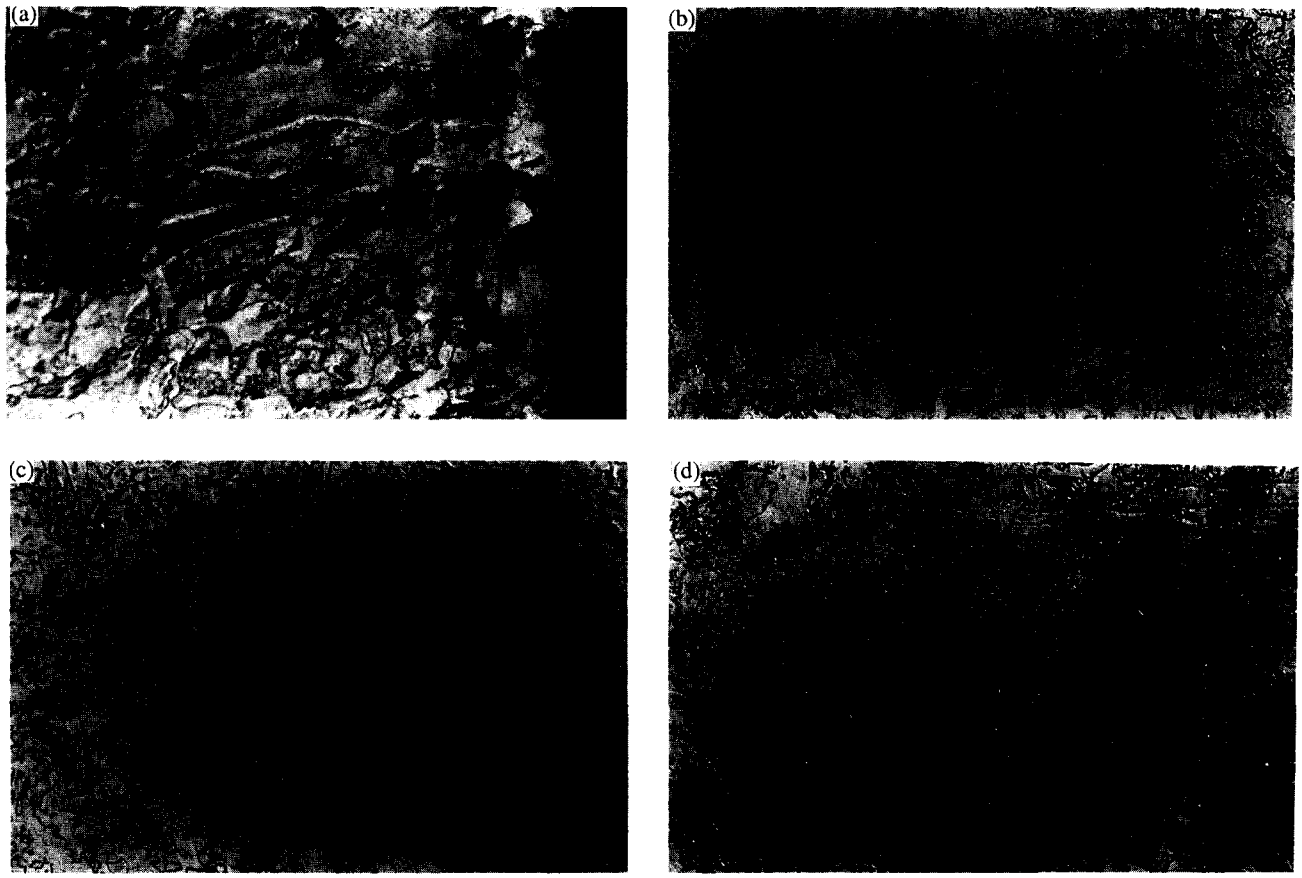

Fig. 1. Metallographical cross sections of Pb–Ca–Sn alloys (primary lead). Mag. ×236: (a) S_1; (b) S_2; (c) S_3; (d) S_4.

discontinuous transformations. With a hot mould, the hardening process starts during cooling and continues immediately after quenching. In this case, an increase in the number of initiation sites of discontinuous transformation is obtained and leads to a refining of the transformed structure, see Fig. 2(d).

The hardness values of the gravity-cast grids (G_1–G_5), reported in Table 1, indicate a weak increase between G_1 and G_2. For higher tin contents, the values remain constant. Concurrently, the puzzling of the structure decreases progressively.

Figs. 3 and 4 show clearly the influence of tin content on the mechanical properties of rolled alloys before expansion. The following is observed:

(i) for less than 0.3 wt.% Sn, the ultimate strengths are low (< 40 MPa) and the elongations are high and do not evolve with time;

(ii) when the tin content exceeds 0.7 wt.%, the mechanical properties are improved, with strengths higher than 50 MPa and weak elongations.

3.2. Corrosion behaviour of Pb–Ca–Sn alloys at 1.5 V

For cast grids (G_1–G_5), the corrosion tests reveal a minimum of weight loss at about 1.2–1.3 wt.% Sn. Corrosion is mainly localized along the grain boundaries. By comparison, expanded grids are corroded uniformly, even at the grid junctions, but the relative weight losses are more important (Fig. 5) and decrease with the level of tin.

With the strips of the S series, containing the same amount of tin (0.6 wt.%), the corrosion is inter-granular and is linked closely to the alloy structure. Thus, with samples having equiaxial grains and a great puzzling (mould at 200 °C), the corrosion appears more regular (S_8). By contrast, for the sample with a basaltic structure (S_5) (Fig. 2(a)) a deep penetration along the grain boundaries can be observed. This region was characterized by microprobe analysis and a high enrichment of tin (1.5 wt.%) was detected in the grain boundaries.

A compact layer of PbO is systematically observed on the alloy surface and, from an analysis performed on the alloy S_5, it appears that the stoichiometry is almost perfectly related to PbO with an homogeneous concentration of tin. From the analysis of ten different points of the layer, the stoichiometric formula obtained for the oxide is $Pb_{1\pm0.07}O_{1\pm0.07}$. Concerning the tin content, it was found that in the bulk of the oxide layer (far from the grain boundaries), the concentration is similar to that found for the alloy itself, viz., 0.70 ± 0.14 wt.%. Finally, in the regions of the oxide closer to the grain boundaries, an intermediary concentration

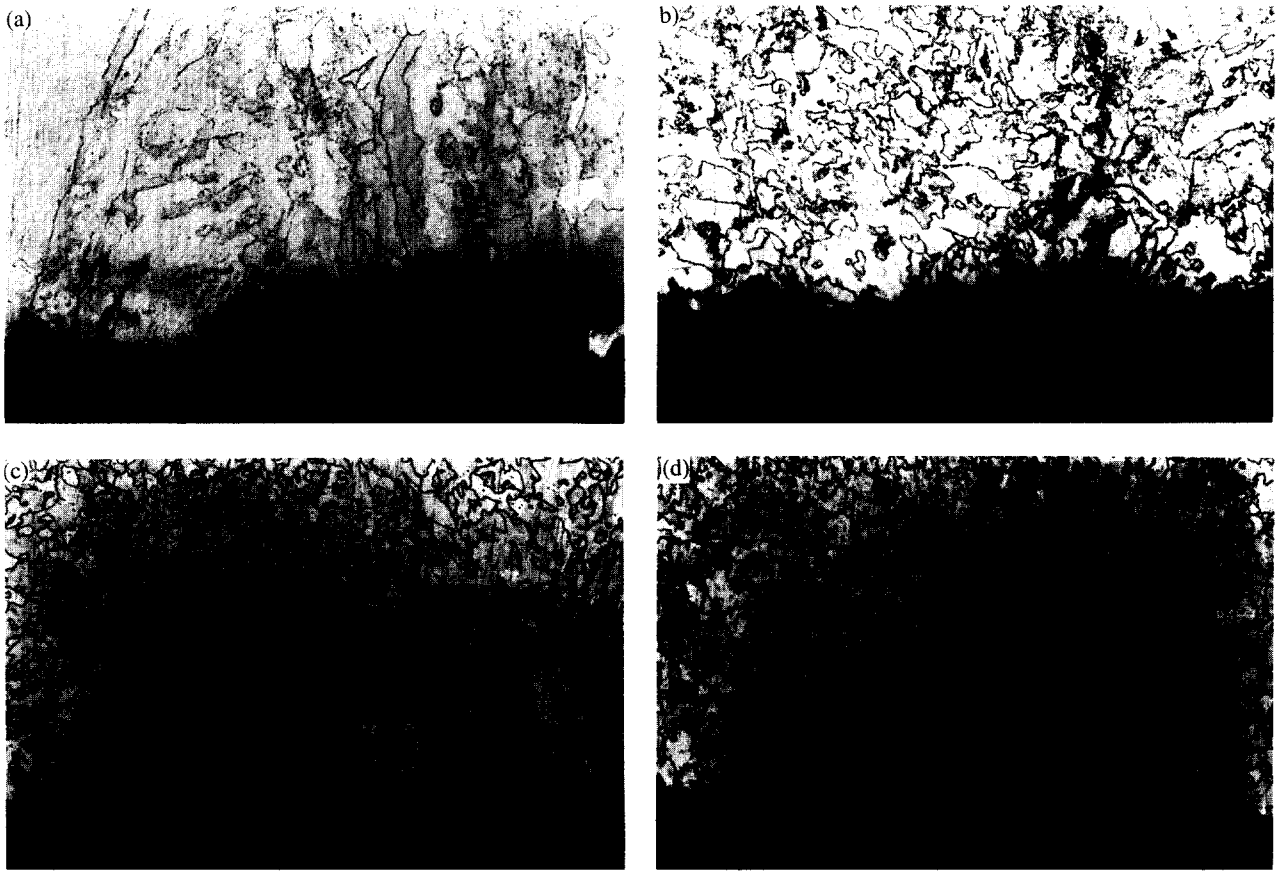

Fig. 2. Metallographical cross sections of Pb–Ca–Sn alloys (secondary lead) after the accelerated corrosion test. Mag. ×236: (a) = S_5; (b) = S_6; (c) = S_7; (d) = S_8.

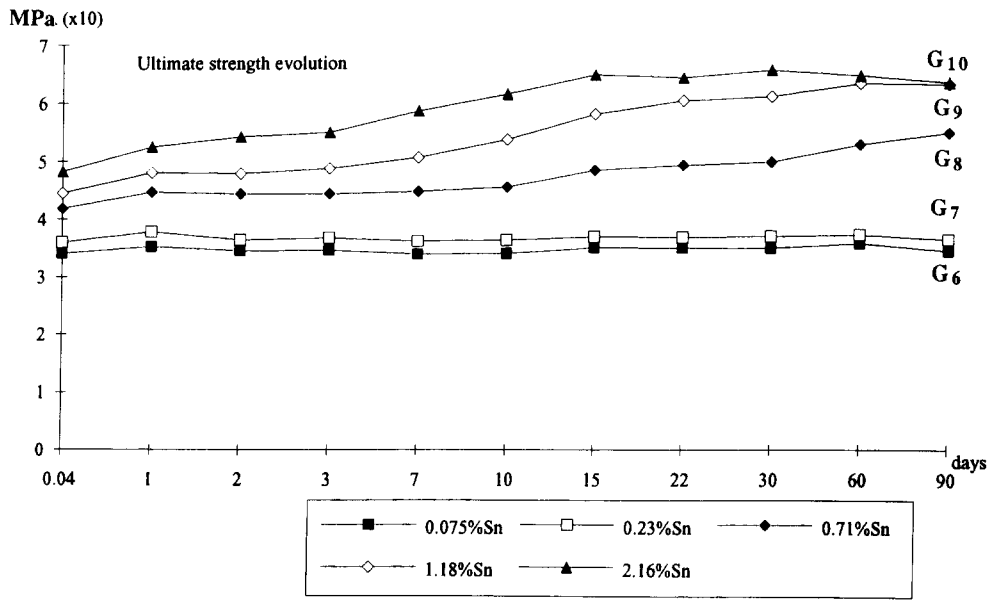

Fig. 3. Ultimate strength of rolled alloys with time (G_6–G_{10}).

of tin is present (≈1 wt.%). This suggests that a certain enrichment was already occurred in these regions.

An outer and thick PbO_2 layer is formed on the inner PbO lead oxide. This layer is, however, not as compact as PbO. The adhesion of the PbO_2 layer is lower by comparison with that of PbO since an appreciable quantity of PbO_2 is found in the experimental cell. The oxide contains mostly the polymorph α-PbO_2; β-PbO_2 is rarely observed and $PbSO_4$ is detected only

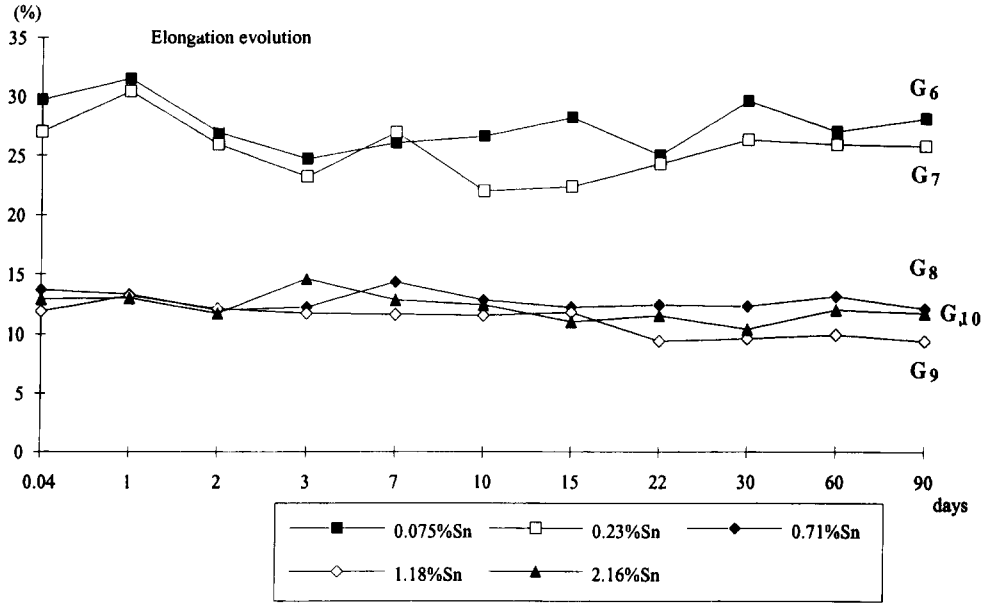

Fig. 4. Elongation of rolled alloys during traction tests with time.

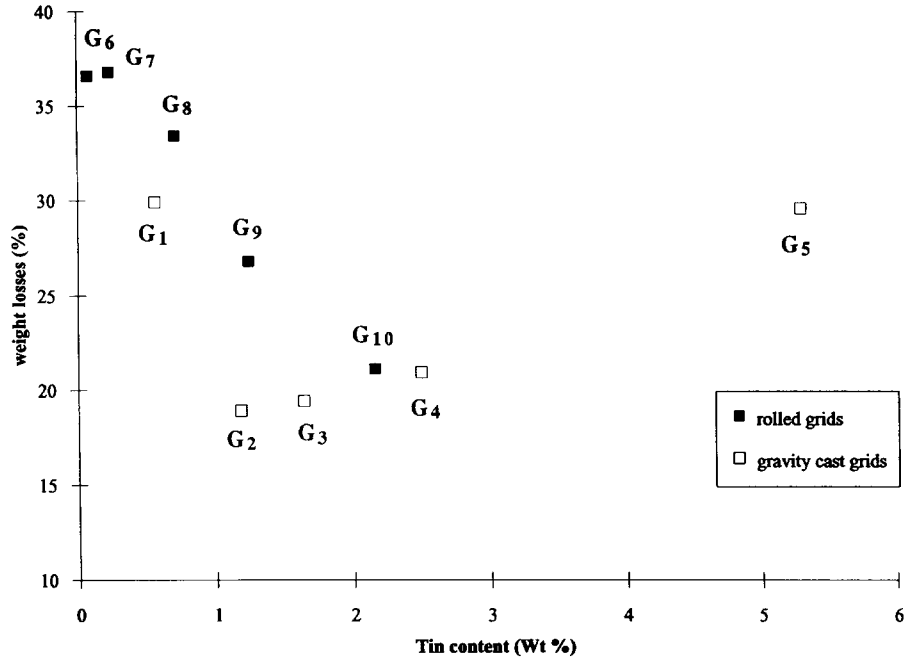

Fig. 5. Accelerated corrosion test on Pb–Ca–Sn grids (G_1–G_{10}) in 5 M H_2SO_4 at 50 °C and at an applied potential of 1.5 V during 7 days.

when the samples are not rinsed and dried quickly after the anodization treatment.

3.3. Corrosion behaviour of Pb–Ca–Sn alloys at 0.7 V

Results of tests performed on the grids reveal the role of tin on the interface passivation. The *R* and *C* values of both cast and expanded grids decrease when the tin content is increased and reach minima for tin contents close to 1 and 2, respectively (Figs. 6 and 7). It should be pointed out that these thresholds are the same as those detected in the accelerated corrosion tests (Fig. 5).

For longer time tests, corrosion gives rise to the growth of a duplex oxide coating that consists of an outer and thin $PbSO_4$ film and a regular inner layer of tetragonal PbO (α-PbO). The metallographical cross section in Fig. 8 is representative of these samples, all characterized by remarkably regular interfaces (Pb/PbO, PbO/$PbSO_4$), without defaults such as cracks, holes. On the other hand, PbO is systematically doped by tin. The tin content in the PbO layer appears to be homogeneous and is closely related to the one in the alloy. Nevertheless, it weakly increases at the Pb/PbO interface (Fig. 9). Finally, the thickness of the PbO

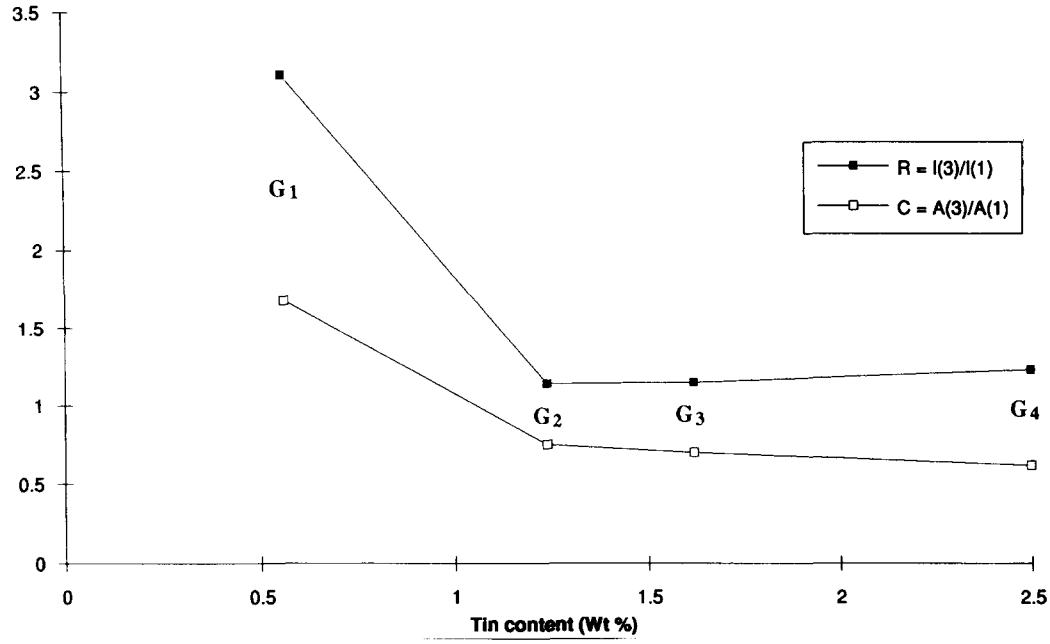

Fig. 6. Development of R and C values for gravity-cast grids with tin content.

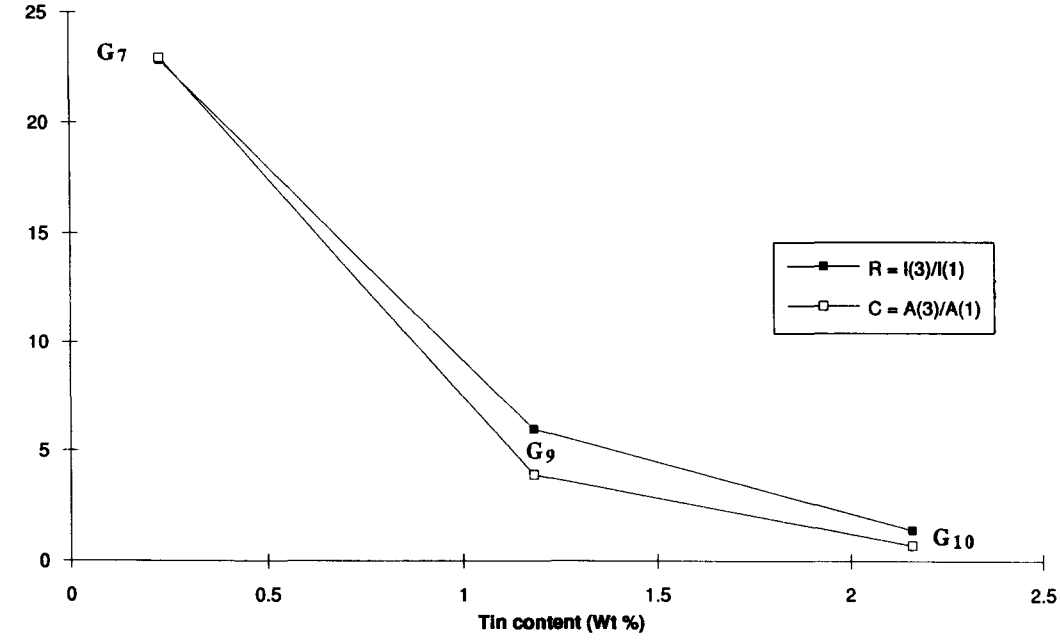

Fig. 7. Development of R and C values for rolled grids with tin content.

layer is continuously reduced by increasing the tin level. A sample with 5 wt.% of Sn was also anodized at 0.7 V during 7 days. In this case, a PbO layer was not detected.

4. Discussion

The evolution of microstructures and mechanical properties depends on the weight ratio of tin:calcium [3–6]. After rapid cooling of the lead alloys, the matrix is over saturated, and this is suitable for age hardening at room temperature.

Category 1. For low values of the tin:calcium ratio, smaller than 3, the alloys exhibit the same behaviour as that observed in binary Pb–Ca alloys with three successive discontinuous transformation stages, i.e.,

(i) an initial fast transformation with regular motion of a rectilinear reaction front achieved in 30 min;

(ii) a second tranformation with an irregular motion of the grain boundaries (called 'puzzling'), and achieved in 24 h;

(iii) a third incomplete reaction, occurring between 48 h and one month, and characterized by a lamellar

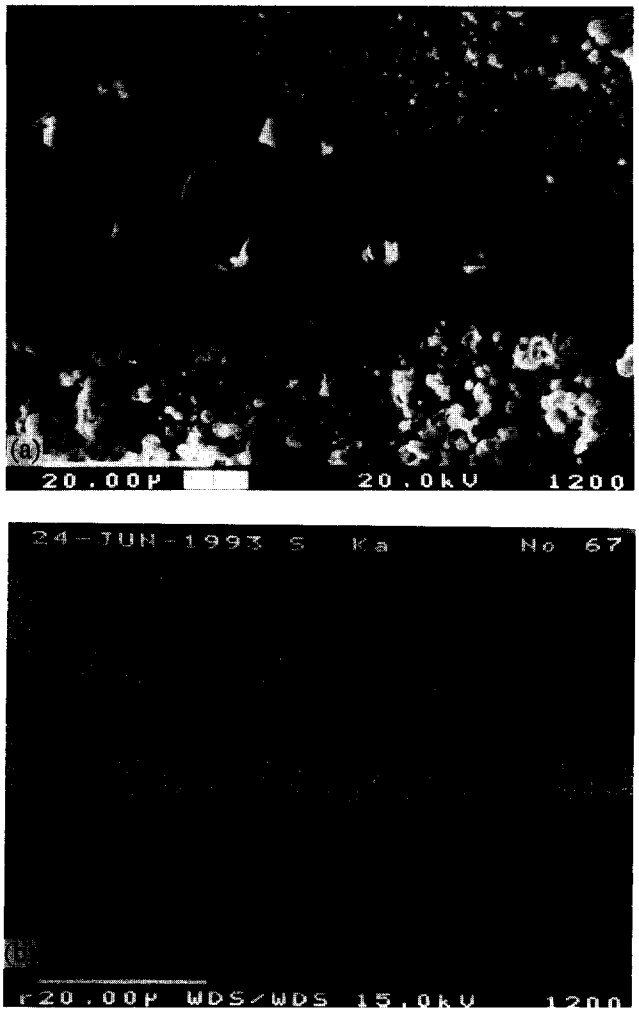

Fig. 8. (a) Metallographical cross section; (b) X image of sulfur. Pb–Ca–Sn alloy after a corrosion test in 0.5 M H_2SO_4 at 20 °C and an applied potential of 0.7 V during 5 days.

precipitation of the Pb_3Ca phase ($L1_2$) in the vicinity of the grain boundaries (overageing).

Category 2. With a high tin:calcium ratio, better than 9, there is only continuous bulk precipitation of the $(Pb_{1-x}Sn_x)_3Ca$ phase, with the $L1_2$ structural type, which starts after an incubation period. During this period, the metal can be rolled and expanded before hardening [7,8]. Finally, a very high level of tin (>2 wt.%) can induce a new discontinuous transformation (overageing) related to the following reaction:

$\alpha Pb + [(Pb_{1-x}Sn_x)_3Ca + Sn]$

(finely dispersed precipitates) ⟶

$\alpha Pb + [(Pb_{1-x}Sn_x)_3Ca + Sn]$

(large and lamellar precipitates)

The presence of three phases is consistent with the Pb–Sn–Ca solid phase equilibria diagram [9] and microprobe analysis.

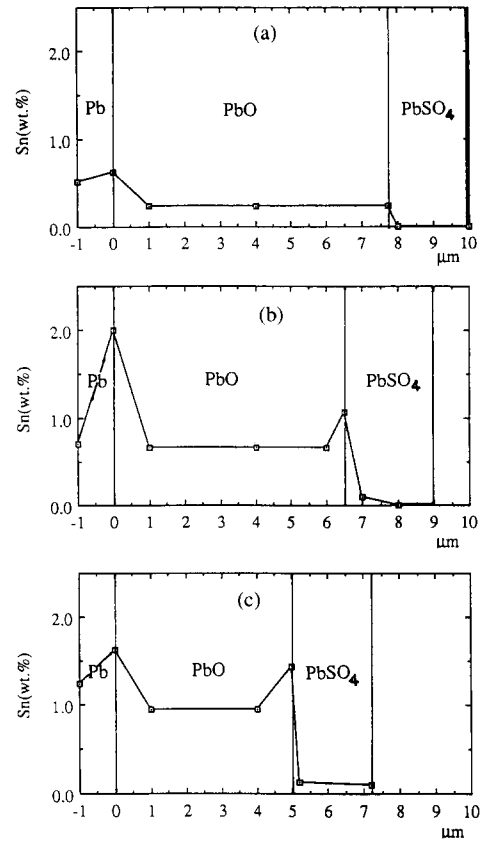

Fig. 9. Tin profiles, determined by EPMA, in PbO layers developed on rolled alloys after 5 days at 0.7 V in 0.5 M H_2SO_4 at 20 °C: (a) G_7 (Pb–0.075wt.%Ca–0.23wt.%Sn); (b) G_8 (Pb–0.075wt.%Ca–0.71wt.%Sn); (c) G_9 (Pb–0.075wt.%Ca–1.18wt.%Sn).

Category 3. For intermediate values of the tin:calcium ratio, four successive transformations (often incomplete) take place, namely:

(i) a linear discontinuous transformation;

(ii) a 'puzzling' transformation;

(iii) a continuous precipitation of $(Pb_{1-x}Sn_x)_3Ca$ in the bulk;

(iv) a discontinuous reprecipitation of lamellar $(Pb_{1-x}Sn_x)_3Ca$ limited to the neighbourhood of the grain boundaries.

According to the above three classifications, G alloys (G_1, G_6 and G_7 excepted) belong to the second group (high Sn/Ca ratio), and are hardened by a continuous coherent bulk micro-precipitation after an incubation period of a few days at 20 °C. In this case, rolling does not hinder hardening and the mechanical properties of the two types of alloys (cast or expanded) are similar; there are only changes in the microstructure.

The G_1 alloy has an intermediate Sn/Ca ratio (category 3), but its hardness reaches a relatively high value. The G_6 and G_7 alloys, with low Sn/Ca ratio, are less hardened. These latter two alloys have been cold worked immediately after casting. During rolling and after, the oversaturated matrix becomes unstable. Thus, two mechanisms can occur: precipitation and recrystallization.

The former increases the hardness while the latter decreases it. In the present case, recrystallization is predominant due to an important deformation (90%) and both hardness and the ultimate strength are low. As a consequence, for a same Sn/Ca ratio, cast and expanded grids present very different metallographic structures and mechanical properties and this prohibits the use of such expanded grids. They are too sensitive to creep.

Concerning alloys of the S series, that all possess an intermediate Sn/Ca ratio (category 3), the lack of any influence of lead purity on hardness or microstructure can be explained if it is remembered that fundamental mechanisms of ageing and recrystallization are not modified by impurities present in secondary lead [3–6]. For this alloy series, it was also observed that the metallographic structure could be influenced greatly by the mould temperature.

Corrosion at 1.5 V, essentially intergranular under overvoltage conditions, will be also dependent on the initial thermal treatment. It is deeper in S alloys with great basaltic grains, but more regular in those with equiaxial grains and significant puzzling (mould at 200 °C). The influence of structure is also detected when both cast and expanded alloys are compared at the same tin level. Corrosive weight loss is more important on the fine-grained, expanded grids and confirms the results of Kelly et al. [10]. In addition, the weight loss passes through a minimum at about 1.3 wt.% Sn for the cast grids and is weakly superior ($\approx$2%) for the expanded ones. These results have been reported previously [11]. With increase of tin, the puzzling structure becomes more and more coarse and the grain boundary areas decrease. This induces less weight loss but more deep inter-granular corrosion. Beyond this minimum, only the cast structure is present (no discontinuous transformation) and corrosion occurs mainly at the dentritic boundaries. This leads to an increase in weight loss. On the other hand, PbO, systematically enriched with tin, has also been detected on the S alloys, between the substrate and α-PbO_2.

With corrosion tests at 0.7 V, PbO with the tetragonal structure is the preponderant compound in the corrosion products that grow under passivation conditions. Both the PbO thickness and the doping level of tin, strongly depend on the tin content in the alloy. These results are consistent with those of Giess [1] that show that by adding 0.2 to 0.4 wt.% Sn to the lead, the extent of the corrosion at 1.0 V versus Hg/Hg_2SO_4 is reduced by a factor of 6–8 and the formation of α-PbO is greatly suppressed [1]. When the tin content reaches about 1 or 2 wt.% (for cast and expanded alloys, respectively), there is a large decrease in the passivation phenomenon. The shift between the two minima is perhaps due to a more regular distribution of the 'active element' in the rolled structure than in the cast one. It can be concluded that tin enrichment at the grain boundaries in the cast alloys induces, during the anodization treatment, a local high level of tin in the lead monoxide. As a consequence, the amount of tin that is able to suppress the passivation is slightly decreased. In all cases under these passivation conditions, the only products detected by XRD are $PbSO_4$ (external) and α-PbO (inner).

Thermodynamically tin is incorporated into the PbO layer as Sn^{4+} [12], either in fine tin oxide precipitates (binary or ternary), or in the PbO lattice. In the former, alternative oxides (such as SnO_2) could improve the electronic conductivity of the corrosion layer by constituting short-circuits while, in the latter, the PbO electronic properties should be modified by doping [13]. Supplementary experiments, using ^{119}Sn Mössbauer spectrometry, are in progress to determine which form of tin is present in the PbO layer. The decrease in the α-PbO thickness when the tin content is increased may be linked to the high acidity of Sn^{4+} that is incompatible with the stability of the lead monoxide, according to the mechanism advanced by Rüetschi [14].

Acknowledgement

The authors thank the European Economic Community that has supported part of this study with the MA2R programme and the Brite EuRam II programme of the Advanced Lead–Acid Battery Consortium.

References

[1] H.K. Giess, in K.R. Bullock and D. Pavlov (eds.), *Proc. Symp. Advances in Lead–Acid Batteries,* Proc. Vol. 84-14, The Electrochemical Society, Inc. Pennington, NJ, USA, 1984, pp. 241–251.
[2] P. Pouchou, *Rech. Aerosp., 3* (1984) 167–192.
[3] L. Bouirden, *Thèse d'Etat,* Université de Nancy I, France, 1990.
[4] L. Bouirden, J.P. Hilger and J. Hertz, *J. Power Sources, 33* (1991) 27–50.
[5] J.P. Hilger (ed.), *Structural Transformations in Lead Alloys,* short intensive training course COMETT, Nancy, France, Mar. 25 and 26, 1993), Laboratoire de Thermodynamique Métallurgique, Université de Nancy I, France, ISBN 2 9505958-3-9.
[6] J.P. Hilger, *Mater. Technol., 6–7* (1993) 33–40.
[7] H. Borchers and H. Assmann, *Metallwiss. Tech., 33* (1979) 936–941.
[8] G. Clerici, *J. Power Sources, 33* (1991) 67–75.
[9] J. Hertz, C. Fornasieri, J.P. Hilger and M. Notin, *J. Power Sources, 46* (1993) 299–310.
[10] D. Kelly, P. Niessen and E.M.L. Valeriotte, *J. Electrochem. Soc., 132* (1985) 2533–2538.
[11] N. Bagshaw, *Power Sources 12, 16th International Power Sources Symp.,* International Power Sources Symposium Committee, Leatherhead, UK, 1988 pp. 113–129.
[12] M. Pourbaix, *Atlas d'Equilibres Electrochimiques,* Gauthier-Villars, Paris, 1963, pp. 475.
[13] D. Pavlov, B. Monakhov, M. Maja and N. Penazzi, *J. Electrochem. Soc., 136* (1989) 27–33.
[14] P. Rüetschi, *J. Electrochem. Soc., 120* (1973) 331–336.